Non-enzymatic glycation increases the failure risk of annulus fibrosus by predisposing the extrafibrillar matrix to greater stresses

Minhao Zhou[1, *]

Erin S. Archibeck[1, *]

Yarah Feteih[1]

Yousuf Abubakr[1]

Grace D. O'Connell[1,2]

[1]Department of Mechanical Engineering

University of California, Berkeley, USA

[2]Department of Orthopaedic Surgery

University of California, San Francisco, USA

*: These authors contributed equally to this work

Submitted to: Acta Biomaterialia

Corresponding Author: Grace D. O'Connell

5122 Etcheverry Hall, #1740,

Berkeley, CA, 94720-1740

Phone: 510-642-3739

Fax: 510-643-5539

e-mail: g.oconnell@berkeley.edu

Abstract

Growing clinical evidence suggests a correlation between diabetes and more frequent and severe intervertebral disc failure, partially attributed to accelerated advanced glycation end-products (AGE) accumulation in the annulus fibrosus (AF) through non-enzymatic glycation. However, in vitro glycation (i.e., crosslinking) reportedly improved AF uniaxial tensile mechanical properties, contradicting clinical observations. Thus, this study used a combined experimental-computational approach to evaluate the effect of AGEs on anisotropic AF tensile mechanics, applying the finite element models (FEM) to complement experimental testing and examine difficult-to-measure subtissue-level mechanics. Methylglyoxal-based treatments were applied to induce three physiologically relevant AGE levels in vitro. Models incorporated crosslinks by adapting our previously validated structure-based FEM framework. Experimental results showed that a threefold increase in AGE content resulted in a ~55% increase in AF circumferential-radial tensile modulus and failure stress and a 40% increase in radial failure stress. Failure strain was unaffected by non-enzymatic glycation. Adapted FEMs accurately predicted experimental AF mechanics with glycation. Model predictions showed that glycation increased stresses in the extrafibrillar matrix under physiologic deformations, which may increase tissue mechanical failure or trigger catabolic remodeling, providing insight into the relationship between AGE accumulation and increased tissue failure. Our findings also added to the existing literature regarding crosslinking structures, indicating that AGEs had a greater effect along the fiber direction, while interlamellar radial crosslinks were improbable in the AF. In summary, the combined approach presented a powerful tool for examining multiscale structure-function relationships with disease progression in fiber-reinforced soft tissues, which is essential for developing effective therapeutic measures.

Keywords: Intervertebral disc; Annulus fibrosus; Advanced glycation end-products; Diabetes; Tissue failure

1. Introduction

Low back pain is a prevalent global health concern affecting 80% of the adult population and is the leading cause of productivity loss, disability, and healthcare expenditures in many regions around the world [1]. The need for improved low back pain management has amplified in recent years, driven by an aging population and the global diabetes epidemic [2-4]. Over the last few decades, there has been a continual increase in global diabetes prevalence, with more than 10% of the world's population being affected [3, 4]. Growing clinical evidence has linked diabetes to intervertebral disc degenerative disorders. Particularly, diabetic patients are ~50% more likely to be diagnosed with disc degenerative disorders, with a longer duration or poorer control of diabetes correlating with a more severe level of degeneration [5-8]. Diabetes is also a significant risk factor for lumbar disc herniation, reportedly increasing its risk by ~50% after correcting for other risk factors such as age, body mass index, lifestyle, and disease history [9].

The intervertebral disc, situated between adjacent vertebrae in the spinal column, is a fibrocartilaginous joint that plays a crucial biomechanical role during daily activities, including supporting multiaxial spinal loads and motions, as well as dissipating energy. The disc is a highly complex, heterogeneous, hierarchical structure comprising a soft gel-like nucleus pulposus center surrounded by a tough, fiber-reinforced annulus fibrosus (AF) ring [10]. Particularly, the AF consists of 15-25 concentric lamellae of angle-ply collagen fibers embedded in a hydrated proteoglycan-rich extracellular matrix, resulting in excellent load-bearing and energy absorption capacities [10]. However, the disc is highly avascular with limited self-healing capabilities; thus, the heavy biomechanical demand placed on the disc makes the AF highly susceptible to catabolic tissue remodeling with degeneration and disease [11, 12]. Such catabolic remodeling has been

shown to initiate, aggravate, or predispose the AF and surrounding structures to irreversible mechanical damage (e.g., tears and disruption), causing debilitating low back pain [11, 12].

A well-documented diabetes-induced structural remodeling in the AF is the accelerated formation and accumulation of advanced glycation end-products (AGE) via non-enzymatic glycation [13-15]. AGEs are a heterogeneous group of chemical compounds that can form irreversible crosslinks with extracellular proteins [13, 15]. The highly collagenous AF is particularly susceptible to AGE modification due to the minimal biological turnover and extended half-life (up to ~120 years) of collagen fibers [16, 17]. Understanding the AF structure-function relationship with non-enzymatic glycation can provide valuable insight into disc mechanical failure mechanisms in diabetic patients, which is pivotal for developing effective therapeutic interventions for tissue failure prevention.

Previous in vitro studies examining the effect of non-enzymatic crosslinks on AF uniaxial tensile mechanics have reported increased tissue stiffness and energetic toughness along the evaluated loading directions [18, 19]. Likewise, our recent work, which was the first to investigate AF uniaxial tensile mechanics at physiologically relevant AGE levels, reported that glycation significantly increased AF tensile modulus, failure stress, and energetic toughness in the circumferential-axial direction (**Figure 1A** – 'Circ-ax specimen') [20]. Joint-level disc mechanics evaluations from studies that induced in vitro crosslinking or used diabetic rodent models fed by AGEs-rich diets also reported higher joint stability and stiffness [21-25]. Therefore, while clinical observations report more frequent and severe tissue failure with AGE accumulation, in vitro mechanical testing results suggest improved tissue mechanical properties with non-enzymatic crosslinking, leaving the relationship between AGE accumulation and tissue failure unclear.

The knowledge of crosslinking structures at the subtissue scale remains limited due to experimental limitations, despite considerable efforts to investigate the functional role of AGEs. Previous work has developed a constitutive relationship to describe AF uniaxial tensile mechanics with non-enzymatic glycation. Still, the relationship was limited to the two-dimensional space and one sample orientation [18]. Finite element models (FEMs) can predict hard-to-measure stress-strain distributions in complex fiber-reinforced tissues. Through combined experimental-FEM study designs, our previous work successfully used FEMs to guide experimental studies and corroborate experimental hypotheses [26, 27]. Additionally, we have developed and validated a multiscale structure-based FEM framework for the AF, which is able to investigate multiscale structure-function relationships in healthy and degenerated AF tissues under various loading and boundary conditions [28-31]. This framework also has the potential to be adapted to describe AF mechanics with non-enzymatic glycation.

Thus, the current study aimed to examine the effect of AGEs on anisotropic AF uniaxial tensile mechanics through a combined experimental-computational approach. To achieve this, we evaluated the impact of AGEs on AF uniaxial tensile mechanics on formerly unexamined orientations (circumferential-radial and radial directions). We also adapted our previous multiscale structure-based FEM framework to describe AF mechanics with crosslinking. The validated model was applied to examine subtissue-level stress-strain distributions, aiming to provide mechanistic explanations for premature tissue failure observed with AGE accumulation. Compared to past AGE-oriented AF mechanics studies, the current study was the first to use a combined experimental-FEM approach, which allowed assessment of subtissue-level stress-strain distributions that are difficult to determine directly through bulk tissue experiments. The validated models provided valuable insight into the effect of AGEs at the subtissue scale, including the likely

orientation of crosslinking structures and extrafibrillar matrix stress distributions. We hypothesized that the improved bulk AF mechanical properties with non-enzymatic glycation were achieved at the risk of exposing the extrafibrillar matrix to increased damage accumulation through mechanical failure and catabolic remodeling.

2. Materials and methods

2.1 Experimental testing

2.1.1 Sample preparation

Bovine discs were used due to their improved accessibility and comparable size, mechanical properties, matrix structures, and biochemical composition to human discs [32-35]. Fresh, skeletally mature, healthy bovine caudal spine sections were acquired from a local butcher (age = 18-24 months; n = 10 spines). Musculature around the discs was removed using a scalpel to prepare disc specimens from C2 to C5 (n = 30 discs). AF specimens oriented in the circumferential-radial and radial directions were prepared from the freshly dissected discs (**Figure 1A** – 'Circ-rad specimen' and 'Radial specimen'). A freezing stage microtome was used to obtain 2 mm-thick rectangular specimens. A custom-built cutting tool was used to ensure a specimen width of 5 mm, while sample length depended on the specimen orientation, with an average of 10 mm for circumferential-radial and 5 mm for radial samples. Both circumferential-radial and radial specimens contained ~10-15 lamellae. To ensure repeatable midlength failure, a 1 mm thick, full-width notch was created using a custom-made cutting jig in the specimen thickness direction for the circumferential-radial samples [26]. Preliminary testing showed that radial specimens exhibited limited grip failure. Thus, the radial specimens were unnotched. Previous studies reported no significant differences in stiffness or strength between notched and intact fiber-

reinforced soft tissue specimens and demonstrated a limited effect of stress concentrations at the notch site [36].

Circumferential-radial specimens were prepared with one of the following three soaking protocols to obtain physiologically relevant AGE levels in vitro. Samples in the control group (CTRL) were soaked for 18 hours at 25 °C in a solution containing 5% phosphate-buffer solution and 5%w/v polyethylene glycol (i.e., SPEG5 solution) to minimize excessive tissue swelling [20, 27]. Glycated samples were soaked in 0.3 M methylglyoxal at either 25 °C (GLY25) or 50 °C (GLY50) [20]. All soaking solutions were pH-balanced to 7.4, and previous work showed that incubation at 50 °C did not alter bulk AF mechanics or composition [34]. Only CTRL and GLY50 groups were prepared for radial specimens, which had collagen fibers oriented perpendicular to the loading direction, resulting in minimal fiber engagement.

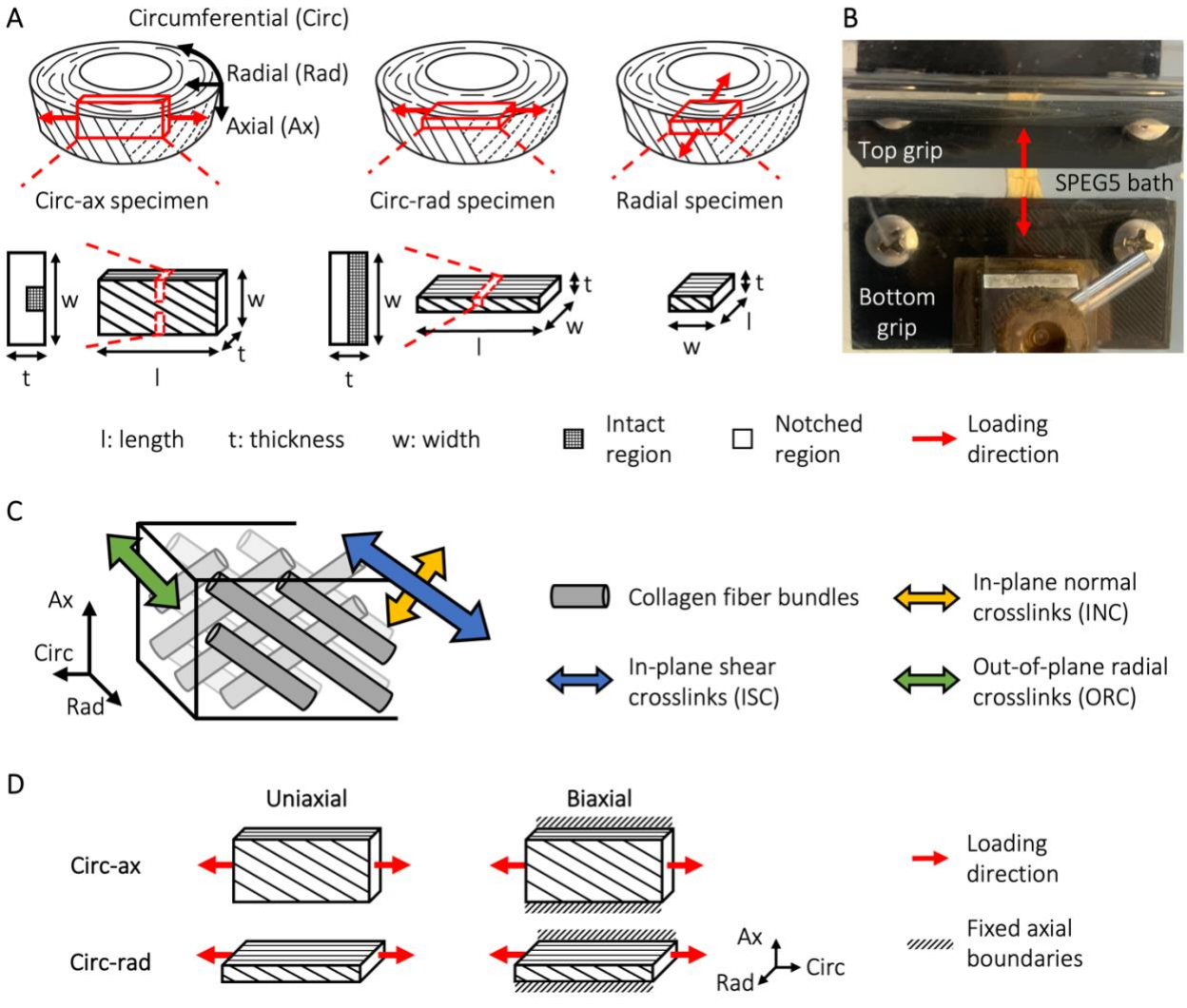

Figure 1: (A) Schematics of specimen orientation, loading direction (red arrows), and midlength notch geometry for the experimental specimens and validation FEMs. **(B)** Circumferential-radial sample gripped by the custom-made serrated screw-clamp grips and soaked in an SPEG5 bath during testing. Red arrows represent the loading direction. Model schematics demonstrating **(C)** possible crosslink orientations and **(D)** simulated uniaxial and biaxial boundary conditions. The models in **(D)** were developed to examine multiscale AF mechanics under the uniaxial and biaxial boundary conditions and were created without a midlength notch.

2.1.2 Mechanical testing

159 Samples were gripped for mechanical testing using a pair of custom-made serrated screw-
160 clamp grips and were placed in a SPEG5 solution water bath to maintain physiologic tissue
161 hydration throughout testing (up to ~170 min; **Figure 1B**). A monotonic 0.1 N preload was applied
162 to remove slack from the tissue. Scale bar photographs of each specimen were taken to measure
163 the initial sample-specific length (circumferential-radial specimen: 9.64 ± 1.46 mm; radial
164 specimen: 4.94 ± 1.48 mm). Uniaxial tension was applied monotonically along the circumferential
165 direction for the circumferential-radial samples (n = 15 per treatment group) and radial direction
166 for the radial samples (n = 8 per treatment group) at a quasistatic loading rate (0.1 mm/min,
167 0.017%/sec). Mechanical testing ended when the specimens were separated into two pieces with
168 no load-bearing capability. Rate-dependent differences were assessed for the circumferential-
169 radial specimens at a high loading rate (50 mm/min, 8.33%/sec, n = 17 per treatment group).
170 Preliminary testing showed that rate-dependent mechanics variations for these specimens followed
171 a similar trend to that reported for the circumferential-axial samples [20]. Since the objective of
172 the current study was to investigate the effect of AGEs on anisotropic AF uniaxial tensile
173 mechanics, high-rate mechanics data are only presented in **Supplementary igure 1**. Unless
174 otherwise specified, the remainder of this article presents mechanical testing data obtained at the
175 quasistatic loading rate.

176 For each specimen that demonstrated a clean midlength failure, engineering stress-strain
177 response was analyzed to facilitate comparison to the existing literature. Engineering stress was
178 calculated as the measured force divided by the initial cross-sectional area evaluated at specimen
179 midlength. Engineering strain was calculated as the tester crosshead displacement divided by the
180 initial gauge (specimen) length. Bulk tensile modulus was calculated at the linear region to ensure
181 physiologic relevance and facilitate comparison with prior literature. The linear region of the

circumferential-radial specimen was identified using a custom linear regression optimization algorithm. The algorithm excluded the toe and yield regions of the stress-strain response and calculated the linear region by determining the maximum range within the stress-strain response in which the change in slope remained within a selected threshold (5%) for strain increments of 0.75% (**Figure 2A** – inset). Failure stress and strain were recorded at the maximum force during testing. The 'failure energy ratio' was also calculated as the strain energy density up to the point of failure divided by the total strain energy density [20].

2.1.3 Biochemistry

After mechanical testing, a 3 mm biopsy punch was used to extract tissue near the failure sites. Tissue samples were blotted dry using a Kimwipe prior to wet weight measurements. The tissue samples were then lyophilized for 48 hours for dry weight measurements. Water content was calculated as the difference between the wet and dry weight divided by the wet weight. Collagen content was measured using the orthohydroxyprsoline (OHP) colorimetric assay, assuming a 1:7.5 OHP-to-collagen mass ratio [37]. Total fluorescence, which estimated the AGE content, was assessed using a quinine sulfate standard at excitation/emission wavelengths of 370 nm/440 nm and was reported as equivalent nanograms of quinine normalized by tissue dry weight [20]. Biochemistry assessments were conducted on the circumferential-radial specimens.

2.1.4 Statistical methods

A priori power analysis was performed using data reported by Werbner et al. to calculate the necessary sample size to achieve a significance level of 0.05 and a power of 0.95 [20]. Pairwise permutation tests with repeated measures were conducted between treatment groups for all mechanical and biochemical properties, as a few datasets did not pass the Shapiro-Wilk Normality Test. All measurements were reported as mean ± standard deviation since most datasets (> 80%)

followed a normal distribution. Bivariate linear correlations were established between tensile modulus and AGE content and between failure stress and AGE content for the circumferential-radial specimens. Correlation strength was determined based on the correlation coefficient R (weak: $|R| < 0.5$, moderate: $0.50 \leq |R| < 0.70$, strong: $|R| \geq 0.70$). A two-way analysis of covariance (ANCOVA) was performed to compare the regression models for the circumferential-radial specimens in this study to the circumferential-axial regression models reported by Werbner et al. (independent variable: AGE content; fixed factor: specimen orientation) [20]. Significance for the permutation tests and ANCOVA was assumed at $p < 0.05$.

2.2 Finite element modeling

2.2.1 Model development and validation

For this study, we adapted a previously validated multiscale structure-based FEM framework developed for the AF [28]. For brevity, only essential model development details are provided, but the reader is encouraged to refer to the previous paper for additional information. In short, the AF was modeled as a fiber-reinforced composite, where the extrafibrillar matrix and collagen fiber bundles were described as distinct materials occupying separate volumes, and the fiber bundles were described as full-length cylinders uniformly distributed throughout the lamellae and welded to the surrounding matrix (**Figure 1C**) [28, 38, 39]. The geometries and dimensions of the validation FEMs were developed to represent rectangular experimental specimens oriented in the circumferential-axial, circumferential-radial, and radial directions (**Figure 1A**) [20]. Individual AF lamellae were modeled as 0.4 mm thick [40], with collagen fibers orienting at ±35° to the anatomical transverse plane to represent samples prepared from the middle-outer AF [41]. Model geometries also included a midlength notch for the circumferential-axial and circumferential-radial specimens (**Figure 1A**). Circumferential-axial (~950k elements),

circumferential-radial (~850k elements), and radial models (~420k elements) contained five, twelve, and eleven lamellae, respectively, which were consistent with the number of lamellae in experimental specimens. Model material descriptions and boundary and loading conditions were defined in FEBio Studio, and the fully defined FEMs were solved by the FEBio solver [42].

The triphasic mixture theory was applied to describe tissue hydration [43]. Model fixed charge density represented tissue proteoglycan content and was set to −100 mmol/L for the matrix and 0 mmol/L for the fibers [34, 44, 45]. To describe the AF solid phase, the extrafibrillar matrix was modeled as a Neo-Hookean material [29], where the Young's modulus (0.5 MPa) and Poisson's ratio (0.3) were determined based on in vitro AF measurements [46, 47]. Collagen fibers were modeled as a compressible hyperelastic ground matrix substance reinforced by a power-linear fiber description to describe AF nonlinearity and anisotropy. The ground matrix substance was modeled using the same Neo-Hookean material described above. For the power-linear fiber description (**Equation [1])**, β represented the power-law exponent in the toe region, E_{lin} represented the fiber modulus in the linear region, λ_0 represented the transition stretch between the toe and linear regions, and B was a function of β, E_{lin}, and λ_0 ($B = \frac{E_{\text{lin}}}{2}(\frac{{\lambda_0}^2-1}{2(\beta-1){\lambda_0}^3} + \frac{1}{\lambda_0})$. Fiber parameters ($E_{\text{lin}}$ = 60 MPa, β = 4, and λ_0 = 1.09) were determined based on our previously validated models and reported AF fiber bundle mechanical testing data [28, 48].

$$\psi_n(\lambda_n) = \begin{cases} 0 & \lambda_n < 1 \\ \frac{E_{\text{lin}}}{4\beta(\beta-1){\lambda_0}^3}({\lambda_0}^2-1)^{2-\beta}(\lambda_n-1)^{\beta} & 1 \le \lambda_n \le \lambda_0 \\ E_{\text{lin}}(\lambda_n-\lambda_0) + B({\lambda_n}^2-{\lambda_0}^2) + \frac{E_{\text{lin}}}{4\beta(\beta-1){\lambda_0}^3}({\lambda_0}^2-1)^2 & \lambda_n > \lambda_0 \end{cases} \quad \textbf{[1]}$$

To account for potential AGE-modifiable fibrous AF crosslinking structures, non-enzymatic crosslinks were modeled as a combination of three possible components oriented in mutually perpendicular directions, including (1) in-plane crosslinks parallel to the collagen fibers (in-plane shear crosslinks), (2) in-plane crosslinks perpendicular to the collagen fibers (in-plane

normal crosslinks), and (3) out-of-plane crosslinks oriented in the AF radial direction (out-of-plane radial crosslinks; **Figure 1C**). All crosslink components were modeled as extrafibrillar reinforcements described by the power-linear fiber description (**Equation [1]**). Since no previous evidence has pointed towards variations in crosslink mechanics with orientation, all crosslink components were assumed to share identical material parameters. Nonlinear crosslink material parameters (i.e., β and λ_0) were assigned the same values as the collagen fibers, with exception of the crosslink modulus ($E_{\text{crosslink}}$), which was the calibrated parameter in this study. A higher AGE content was assumed to generate a proportionally greater number of AGEs that could crosslink collagen fibers, resulting in denser AGE compounds per specimen unit volume, and thus a higher apparent crosslink modulus (i.e., $E_{\text{crosslink, GLY50}} = 2\times E_{\text{crosslink, GLY25}}$).

The adapted FEM was validated to ensure its predictive power over AF uniaxial tensile mechanics with non-enzymatic glycation. All validation FEMs were loaded in two steps. To account for specimen hydration, free-swelling was simulated in the SPEG5 external bath [27]. The post-swelling, pre-tension configuration was defined as the reference configuration for mechanics calculations. A uniaxial quasistatic tensile ramp to 40% engineering strain was then applied in the circumferential direction for the circumferential-axial and circumferential-radial models, while a uniaxial quasistatic tensile ramp to 150% radial engineering strain was simulated for the radial model. Displacement on the specimen top and bottom surfaces was constrained to the loading direction throughout the simulated tension. For the circumferential-axial and circumferential-radial models, the tensile modulus was calculated as the slope of the linear region of the engineering stress-strain curve between 25% and 35% engineering strain. The tensile modulus for the radial models was calculated as the slope of the engineering stress-strain response between 100% and 150% engineering strain. To ensure an optimal solution for the crosslink modulus

calibration, a parametric study was conducted by developing parametric FEMs with varying crosslink modulus (n = 16 for circumferential-axial and circumferential-radial models). Model predictions were considered valid if the predicted tensile modulus deviated from the respective reported experimental means by less than 50% of the reported standard deviation.

A multivariate linear regression model was used to evaluate the relationship between the increase in AF circumferential tensile modulus and crosslink modulus based on the parametric FEM models. Significance was assumed for $p < 0.05$. The relative contribution of crosslink modulus to the increase in AF circumferential tensile modulus was calculated using the relaimpo package in R and reported as a percentage [49].

2.2.2 Effect of non-enzymatic glycation on multiscale AF mechanics

Following model validation, another set of circumferential-axial and circumferential-radial models was developed to investigate the effect of non-enzymatic glycation on multiscale AF mechanics. While model dimensions still mimicked the samples for mechanical testing, the midlength notch geometry was excluded (**Figure 1D**). Models were developed to represent the CTRL and GLY50 samples loaded under uniaxial and biaxial boundary conditions. For the uniaxial models, the boundary and loading conditions were identical to the validation FEMs. For the biaxial models, the axial boundaries were fixed throughout the simulated quasistatic tension, which was applied in the circumferential direction to 40% engineering strain (**Figure 1D**). The post-swelling, pre-tension configuration was defined as the reference configuration. The apparent bulk tensile modulus was calculated as the slope of the linear region of the engineering stress-strain curve between 25% and 35% engineering strain. The average stress in the extrafibrillar matrix and fibers were evaluated throughout the simulated tension. The percentage of failed tissue elements was evaluated at 0.5 MPa circumferential stress due to physiologic relevance [40], which

was calculated as the applied circumferential load divided by the respective specimen cross-sectional area. To ensure the repeatability of our model predictions, the percentage of tissue failure was also evaluated using a strain-based assumption at 15% circumferential engineering strain, which corresponds to the largest internal AF strain observed in vitro in intact discs under physiologically relevant loadings [50, 51]. Failure of individual tissue elements was assessed using a stress-based criterion. Bulk AF radial failure stress was considered representative of matrix failure stress due to the minimum fiber engagement in that orientation. The failure stress threshold for the fibers was determined based on data in the literature [52]. The failure threshold was set at 75% of the respective mean failure stress to better represent tissue failure initiation following yielding [53].

3. Results

3.1 Experimental testing

Circumferential-radial specimens demonstrated a nonlinear bulk stress-strain response, while radial samples showed a pseudo-linear bulk stress-strain response prior to bulk tissue failure (**Figure 2** – colored solid lines). A clear linear region was observed for all circumferential-radial specimens (**Figure 2A** – inset). A maximum stress that corresponded to bulk tissue failure was observed for all specimens. Mechanical testing data was only analyzed for samples that demonstrated a clean midlength failure (circumferential-radial: 73% of total specimens, n = 11 per treatment group; radial: 88% of total specimens, n = 7 per treatment group).

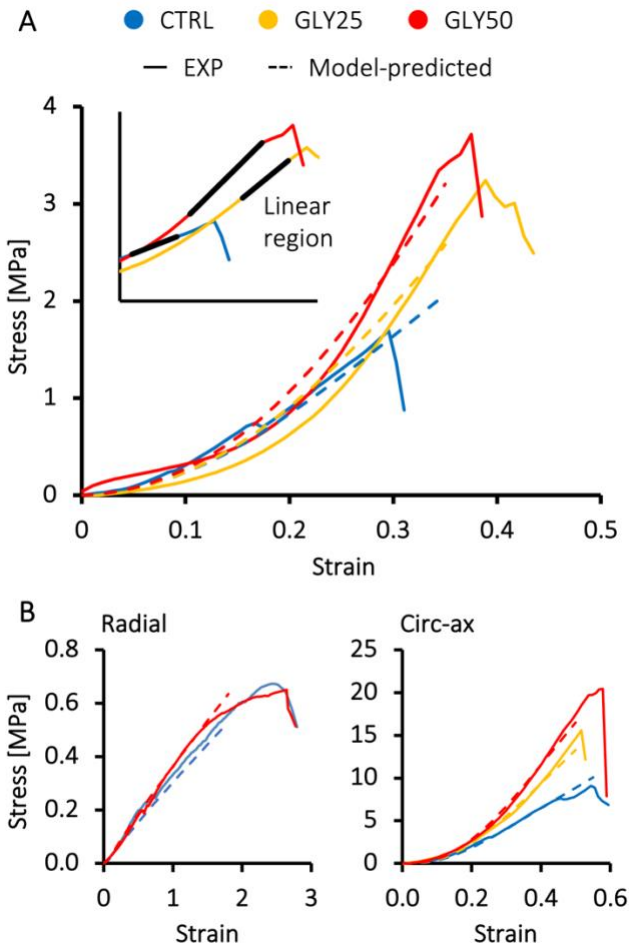

Figure 2: Representative experimental (EXP) and model-predicted engineering stress-strain curves at each glycation level for **(A)** circumferential-radial and **(B)** radial and circumferential-axial specimens. Data reported for circumferential-axial samples were adapted from Werbner et al. for model validation [20]. Inset in **(A)** demonstrates the linear regions calculated by the custom linear regression optimization algorithm using bolded black line segments.

For circumferential-radial specimens, the GLY50 treatment increased the tensile modulus by 53% compared to the CTRL group (CTRL: 11.73 ± 2.76 MPa, GLY50: 17.96 ± 3.24 MPa, $p < 0.001$) and by 35% compared to the GLY25 group (GLY25: 13.33 ± 4.95 MPa, $p = 0.013$; **Figure 3** – Circ-rad). The GLY50 treatment also increased the failure stress by 57% compared to the CTRL group (CTRL: 2.35 ± 0.77 MPa, GLY50: 3.69 ± 0.83 MPa, $p < 0.001$) and by 32%

compared to the GLY25 group (GLY25: 2.79 ± 1.24 MPa, p = 0.012; **Figure 4A** – Circ-rad). However, the tensile modulus and failure stress of the GLY25 samples were not different from the CTRL specimens (p > 0.35). For radial specimens, the GLY50 treatment increased the failure stress by 40% compared to the CTRL group (CTRL: 0.39 ± 0.15 MPa, GLY50: 0.54 ± 0.09 MPa, p = 0.043; **Figure 4A** – Radial). However, the tensile modulus was not affected by the glycation treatment (p > 0.90; **Figure 3** – Radial). Non-enzymatic glycation did not affect tissue failure strain in both tested orientations and all treatment groups (p > 0.35; **Figure 4B**). Additionally, a trend in failure energy ratio was not observed with non-enzymatic glycation.

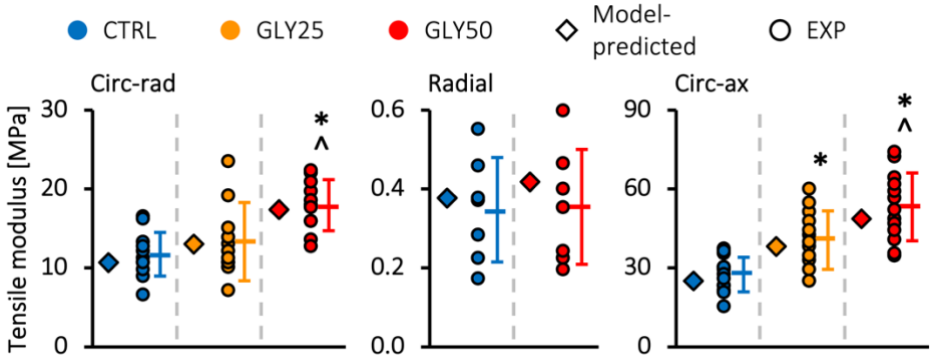

Figure 3: Experimental tensile modulus (circles) compared to model predictions (diamonds) at each glycation level for all three specimen orientations. Data reported for circumferential-axial samples are reproduced from Werbner et al. for model validation [20]. * represents p < 0.001 vs. CTRL; ^ represents p < 0.05 vs. GLY25.

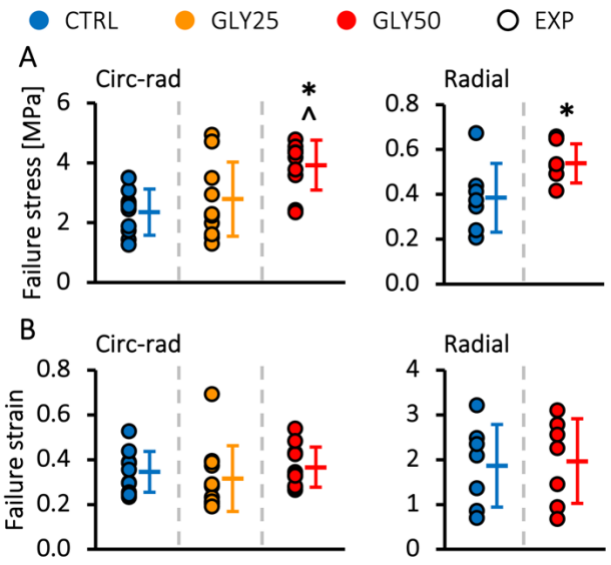

Figure 4: (A) Failure stress and **(B)** failure strain at each glycation level for both specimen orientations. * represents $p < 0.05$ vs. CTRL; ^ represents $p < 0.05$ vs. GLY25.

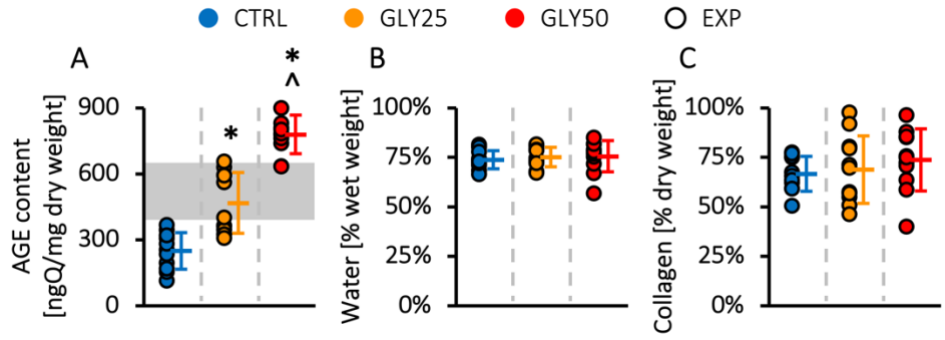

Figure 5: (A) AGE, **(B)** water, and **(C)** collagen content at each glycation level. The gray region in **(A)** represents the range of AGE content measured in human discs [20]. * represents $p < 0.001$ vs. CTRL; ^ represents $p < 0.001$ vs. GLY25.

AGE content normalized by tissue dry weight increased by 87% with the GLY25 treatment (CTRL: 250 ± 84 ngQ/mg dry weight; GLY25: 468 ± 138 ngQ/mg dry weight, $p < 0.001$) and by ~210% with the GLY50 treatment (GLY50: 779 ± 87 ngQ/mg dry weight, $p < 0.001$). The AGE content of the GLY50 group was ~65% higher than the GLY25 group ($p < 0.001$; **Figure 5A**). Water and collagen content were not affected by the glycation treatment (**Figures 5B** and **5C**).

In the circumferential-radial direction, there was a moderate positive correlation between AGE content and tensile modulus ($R = 0.55$, $p < 0.001$; **Figure 6A** – black trendline); a moderate positive correlation was also observed between AGE content and failure stress ($R = 0.55$, $p < 0.0001$; **Figure 6B** – black trendline). Specimen orientation had a significant effect on the relationship between AGE content and tensile modulus and between AGE content and failure stress (ANCOVA $p < 0.001$), with the tensile properties of circumferential-axial specimens being more sensitive to AGE accumulation (**Figure 6** – gray vs. black trendlines).

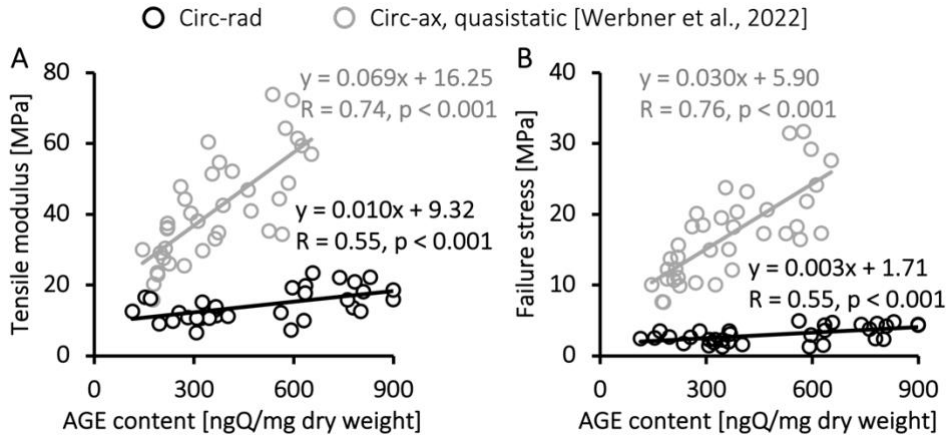

Figure 6: Bivariate linear correlation between **(A)** tensile modulus and **(B)** failure stress and AGE content for circumferential-radial samples (black circles). Quasistatic circumferential-axial data reported by Werbner et al. were shown for comparison (gray circles) [20]. Regression models obtained for the two specimen orientations were significantly different (ANCOVA $p < 0.001$).

3.2 Finite element modeling

3.2.1 Model validation

With all three possible crosslink components (i.e., in-plane shear crosslinks, in-plane normal crosslinks, and out-of-plane radial crosslinks, **Figure 1C**), model predictions showed that a crosslink modulus lower than 0.1 MPa was required to predict an AF radial tensile modulus within the range of existing experimental data (**Figure 7A**). Meanwhile, FEMs with a crosslink

modulus of 10 MPa predicted an AF radial tensile modulus of 6.38 MPa, more than 10× higher than the largest AF radial tensile modulus reported (**Figure 7A**). However, a crosslink modulus greater than 7.5 MPa was required to generate model predictions within around one standard deviation of the mean circumferential tensile modulus values (**Figure 7B**). Therefore, out-of-plane radial crosslinks were not included in the model (**Figure 1C**). Model predictions also showed that FEMs with only in-plane shear crosslinks or in-plane normal crosslinks greatly underestimated AF circumferential tensile modulus for the GLY50 group (**Figure 7C**). Thus, both in-plane shear crosslinks and in-plane normal crosslinks were necessary and therefore included in the model.

Adapted FEMs accurately and robustly predicted experimental measurements when the crosslink modulus was 12.5% of collagen fibers (i.e., 7.5 MPa) in the GLY25 model and 25% of collagen fibers (i.e., 15 MPa) in the GLY50 model, which was further confirmed by the parametric FEM predictions (**Figure 7B**). Model predictions matched well with experimental stress-strain responses in all specimen orientations and all treatment groups (**Figure 2** – colored dashed vs. solid lines). Model-predicted bulk AF tensile modulus values were within 0.4× standard deviation from the experimental means in all specimen orientations and all treatment groups (**Figure 3**). Thus, the adapted FEMs were considered valid for describing and investigating AF tensile mechanics with non-enzymatic glycation.

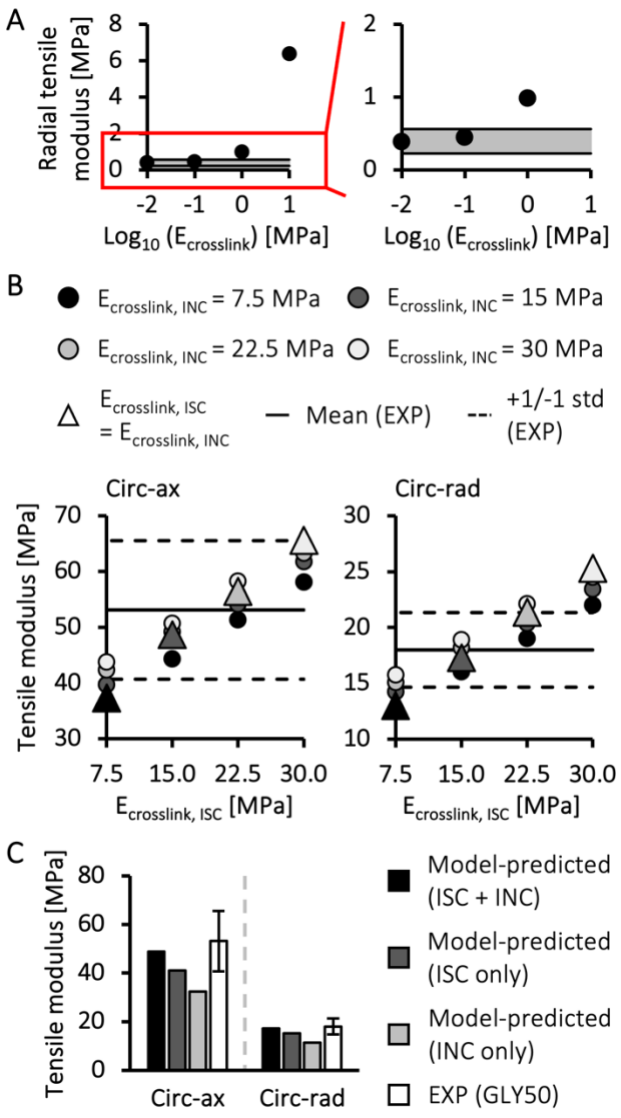

Figure 7: (A) Model-predicted AF radial tensile modulus with varying crosslink modulus ($E_{crosslink}$ = 0.01 MPa, 0.1 MPa, 1 MPa, and 10 MPa). Predicted values were compared to the AF radial tensile modulus range reported in the literature, highlighted by the gray region [40, 54-56]. **(B)** Model-predicted tensile modulus for circumferential-axial and circumferential-radial specimens with varying crosslink modulus. Horizontal solid and dashed lines represent the range of experimental data (mean ± standard deviation, std). **(C)** Model-predicted circumferential tensile modulus for GLY50 specimens with varying crosslinking structures vs. experimental data.

Multivariate linear regression models were able to explain more than 99.5% of the variance in parametric FEMs. Terms associated with the out-of-plane radial crosslinks were excluded from the models. The increase in AF circumferential tensile modulus increased linearly with in-plane shear and in-plane normal crosslink modulus ($p < 0.001$ for both crosslink types and specimen orientations) but did not depend on their interactions (**Equations [2]** and **[3]**). The relative contribution analysis suggested that the increase in AF circumferential tensile modulus was more sensitive to the in-plane shear than the in-plane normal crosslink modulus. Particularly, the in-plane shear crosslink modulus contributed to ~90% of the increase in circumferential tensile modulus in both orientations, while the in-plane normal crosslink modulus only contributed ~10%.

$$\Delta E_{\text{Circ-ax}} = 4.62 + 0.91 \times E_{\text{crosslink, ISC}} + 0.27 \times E_{\text{crosslink, INC}} + \varepsilon \quad \textbf{[2]}$$

$$\Delta E_{\text{Circ-rad}} = 0.21 + 0.41 \times E_{\text{crosslink, ISC}} + 0.13 \times E_{\text{crosslink, INC}} + \varepsilon \quad \textbf{[3]}$$

3.2.2 Effect of non-enzymatic glycation on multiscale AF mechanics

For circumferential-axial models, the biaxial boundary condition increased the apparent tensile modulus by 62-85% (**Figure 8A** – Circ-ax, diagonal vs. solid bars). Glycation had a comparable effect, increasing the apparent tensile modulus by 66-89% (**Figure 8A** – Circ-ax, red vs. blue bars). For circumferential-radial models, the biaxial boundary condition had a less pronounced effect, only increasing the apparent tensile modulus by 17-28% (**Figure 8A** – Circ-rad, diagonal vs. solid bars); however, glycation increased the apparent tensile modulus by more than 75% (**Figure 8A** – Circ-rad, red vs. blue bars).

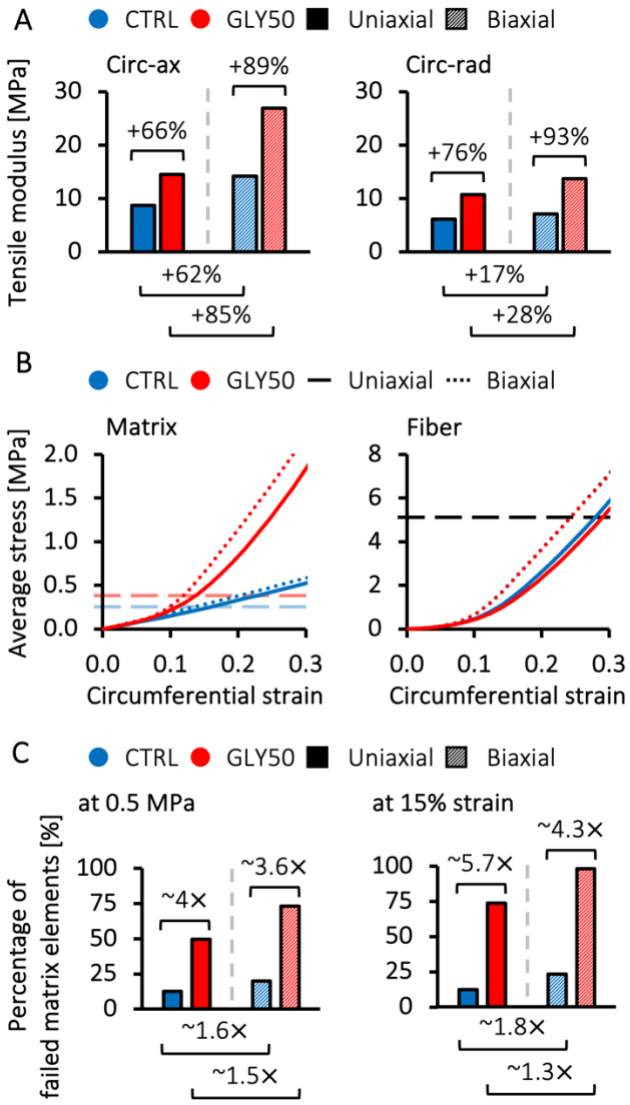

Figure 8: Model-predicted **(A)** circumferential tensile apparent modulus, **(B)** average matrix and fiber stress. The light blue and red horizontal dashed lines represent the stress thresholds for failed matrix elements in CTRL and GLY50 models, respectively. The black dashed line represents the failure stress threshold for fibers [52]. **(C)** Percentage of failed matrix elements evaluated at 0.5 MPa circumferential stress and 15% engineering strain.

Model predictions indicated that glycation had a greater impact on subtissue-level mechanics than altered boundary conditions, especially in the extrafibrillar matrix (**Figures 8B**, **8C**, and **9**). Under 0.5 MPa, the average matrix stress in the uniaxial circumferential-axial CTRL

model was 0.25 MPa and increased by ~60% to 0.40 MPa with glycation (**Figure 8B** – Matrix, solid blue vs. red lines; **Figure 9A**). Simulating a biaxial boundary condition only increased the average matrix stress by less than 5% (**Figure 8B** – Matrix, blue solid vs. dotted lines; **Figure 9A**). Based on the failure criterion calculated using the measured AF radial failure stress (CTRL: 0.39 MPa × 75% = 0.29 MPa; GLY50: 0.54 MPa × 75% = 0.40 MPa; **Figure 4A**), glycation led to a ~4× increase in the percentage of failed matrix elements from 13% to 50% under uniaxial tension at 0.5 MPa (**Figure 8C** – red vs. blue solid bars), while biaxial loading resulted in a ~1.5× increase in the percentage of failed matrix elements (**Figure 8C** – diagonal vs. solid blue bars). In the circumferential-axial biaxial models, glycation increased the average matrix stress by ~90% from 0.30 to 0.56 MPa (**Figure 8B** – Matrix, dotted blue vs. red lines; **Figure 9A**), resulting in over 70% of the matrix elements exceeding the failure threshold (**Figure 8C** – at 0.5 MPa, diagonal red bar). A similar trend was observed when evaluating failure using a strain-controlled assumption at 15% engineering strain (**Figure 8C** – at 15% strain; **Figure 9B**).

Contrary to the changes in matrix mechanics, the average fiber stress was largely unaffected by glycation (**Figure 8B** – Fiber, red vs. blue lines; **Figure 9**). At 0.5 MPa circumferential stress or 15% engineering strain, increasing the boundary constraints with the biaxial boundary increased the average fiber stress by 20-70%, but the average fiber stress remained well below the failure threshold (**Figure 8B** – Fiber, solid vs. dotted lines). A similar trend was observed for models oriented in the circumferential-radial direction.

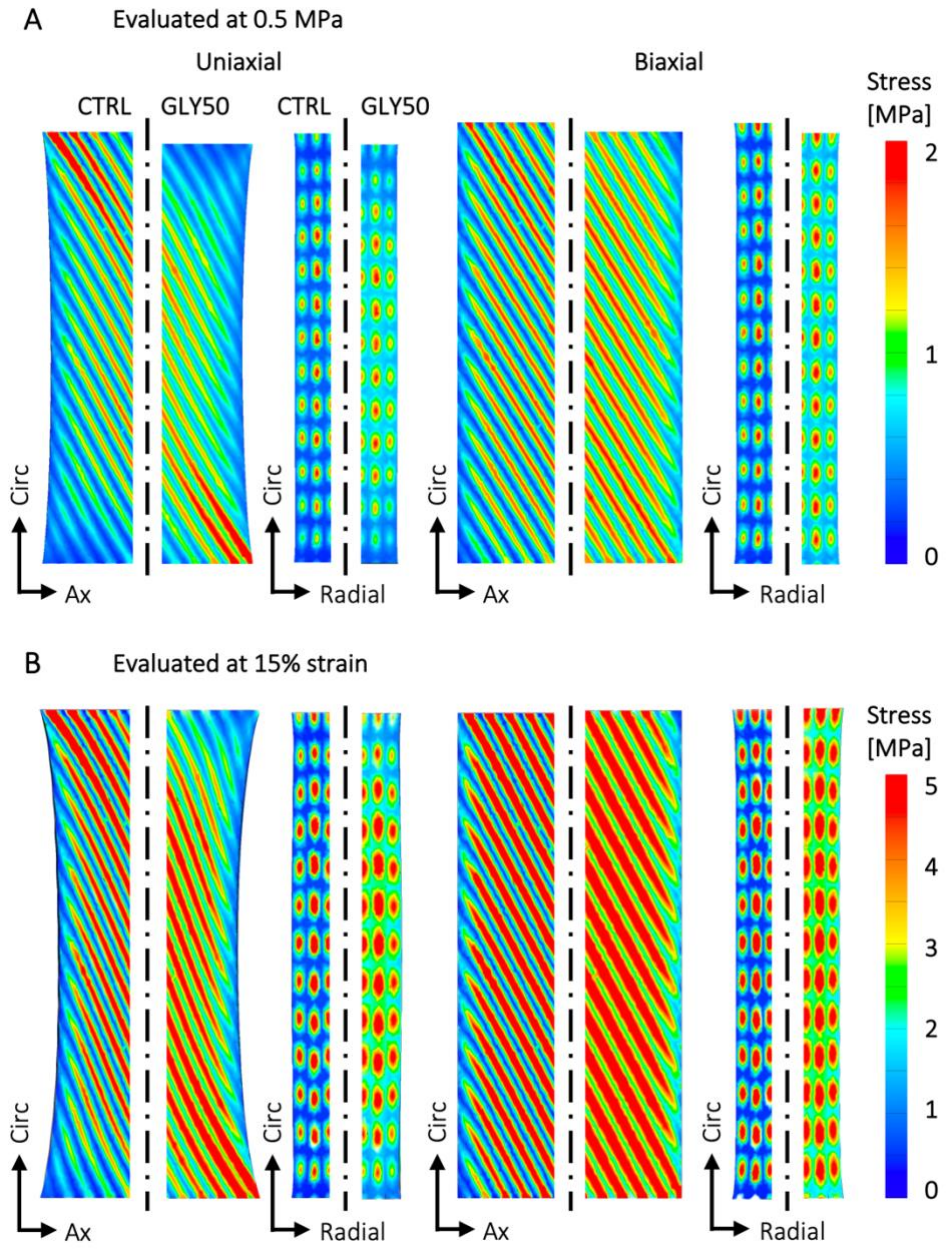

Figure 9: (A) Representative frontal and side midplane stress distributions at 0.5 MPa circumferential stress for CTRL and GLY50 models. Stress in the extrafibrillar matrix increased with glycation, changing from dark blue shading in the CTRL to green in the GLY50 models. Red shadings represent higher stresses in the fibers (vs. the matrix). **(B)** Representative stress distributions at 15% applied circumferential engineering strain showed a similar trend.

Discussion

448 The study investigated the relationship between physiologic levels of advanced glycation
449 end-products and anisotropic AF uniaxial tensile mechanics using a combined experimental-
450 computational approach. In vitro glycation increased AF tensile modulus and failure stress in the
451 circumferential-radial direction (**Figures 3** and **4A**), agreeing with previous observations reported
452 for circumferential-axial samples [19, 20]. However, for circumferential-radial specimens,
453 changes in tensile mechanics with AGE accumulation were not as pronounced (**Figure 6**) [20].
454 Specifically, the in vitro glycation treatments led to comparable increases in AGE content in both
455 specimen orientations [20]. However, the GLY50 treatment increased the AF tensile modulus and
456 failure stress by ~100% for the circumferential-axial specimens but only by ~50% for the
457 circumferential-radial specimens. While the GLY25 treatment led to statistically significant
458 increases in circumferential-axial tensile modulus and failure stress, it did not affect the
459 circumferential-radial specimens (**Figures 3** and **4A**). Additionally, multivariate linear regression
460 predicted that the modulus of in-plane shear crosslinks, which are parallel to the collagen fibers,
461 contributed to approximately 90% of the increase in tensile modulus. The primary distinction
462 between circumferential-axial and circumferential-radial specimens lies in the loading direction
463 relative to the orientation and length of the collagen fibers. In particular, collagen fibers in the
464 circumferential-radial specimen extended across the 2 mm thickness, while fibers in the
465 circumferential-axial sample traversed the entire 5 mm width, resulting in a larger effective fiber
466 length and fiber engagement [29, 57]. Taken together, these findings indicated that non-enzymatic
467 crosslinks had the greatest impact along the collagen fiber direction, with this effect increasing
468 with intact fiber length and fiber engagement.
469 Non-enzymatic glycation had a smaller effect on AF radial mechanics, where fiber
470 engagement was minimal during loading. Specifically, the GLY50 treatment did not affect the

tissue modulus and only increased the failure stress by 40% (**Figures 3** and **4A**). FEM predictions also suggested a negligible effect from the AGEs in the radial direction (**Figure 1C**), as including out-of-plane radial crosslinks led to unrealistically high radial tensile modulus (**Figure 7A**). While defining a smaller modulus for the radial crosslinks (i.e., 0.01-0.1 MPa) compared to the in-plane crosslinks produced realistic AF radial tensile modulus predictions (**Figure 7A**), we did not find previous evidence supporting stiffness variations between AGEs compounds derived from the same collagen type. Previous two-dimensional constitutive models developed to describe AF mechanics with glycation also suggested that in-plane crosslinks were sufficient [18]. Furthermore, elastin proteins, the main constituents of interlamellar elastic fibers oriented in the AF radial direction, only accounted for 2% of tissue dry weight, indicating a low likelihood of elastin-derived AGEs compounds (i.e., out-of-plane radial crosslinks) [58-60]. A multiphoton autofluorescence study further complemented these findings by demonstrating that collagens were more responsive to AGE formation than interlamellar elastic fibers [61]. Thus, our results agree with and add to the existing literature regarding the crosslinking structure by showing that interlamellar radial crosslinks are unlikely to form in the AF.

Studies that evaluate mechanical properties of human disc soft tissues are known to report large variations. While reported mechanics variations between studies can be attributed to differences in specimen geometry [29], variations within studies might, in part, be due to differences in tissue composition with degeneration and disease. For example, coefficients of variation (i.e., the ratio of the standard deviation to the mean) for the tensile modulus of healthy anterior outer circumferential-axial AF specimens, whose structure and morphology are expected to be relatively uniform, still range from 0.56 to 0.82 [53, 55, 56, 62]. This study evaluated a parametric group of crosslink modulus values corresponding to different AGE levels to determine

494 the effect of AGE accumulation on bulk tissue mechanics. The parametric models predicted a
495 range of modulus values that spanned the experimental variations reported in both specimen
496 orientations (**Figure 7B**). This finding suggested that large variations observed in human disc
497 mechanical properties may be in part due to variations in AGE content, which are often not
498 accounted for during tissue degeneration level evaluations (e.g., Thompson scale) [63].

499 AGE accumulation occurs naturally with aging and has been linked to various soft tissue
500 diseases besides disc degenerative disorders, such as osteoarthritis and tendinopathy [15, 64, 65].
501 Studies using diabetic rodent models also reported significantly reduced tendon modulus and
502 failure stress [66, 67]. However, conflicting results have been reported in vitro. In addition to the
503 increased AF energetic toughness reported in the current and previous AF studies [18-20], non-
504 enzymatic glycation in vitro has been found to increase tissue stiffness and failure stress in other
505 soft fiber-reinforced soft tissues, such as tendons, cartilages, and corneas [68-72]. In vitro
506 crosslinking also enhanced tissue resistance to collagen degradation and mechanical wear [73].
507 Researchers have partially attributed this discrepancy to the uncoupling of exogenous AGE
508 accumulation from natural cellular and tissue remodeling in response to a high AGE extracellular
509 environment, which is known to induce cellular inflammatory responses [24, 74-77]. Alternatively,
510 tendon studies reported that AGE treatment significantly reduced tissue viscoelastic properties (i.e.,
511 energy dissipation capabilities) [69, 70], suggesting that diabetic crosslinking might induce
512 premature tissue failure by compromising tissue performance under fatigue loading. Additionally,
513 tendon studies have shown that non-enzymatic glycation may result in tissue stiffening due to
514 diminished interfibrillar sliding [69, 70, 72, 78]. Similar mechanisms may be at play in the AF,
515 despite the differences in tissue composition and fiber orientation; however, interfibrillar sliding
516 was beyond the scope of this study.

In this study, subtissue-level FEM predictions provided another probable explanation for this discrepancy between in vivo and in vitro tissue failure behavior with AGE accumulation. Under a physiologically relevant strain (i.e., ≤ 15% strain) or stress range (i.e., ~0.5 MPa), glycation greatly increased the stress in the extrafibrillar matrix, predisposing a larger portion of the tissue to a greater risk of mechanical failure (**Figures 8B** and **C**). The current study evaluated matrix failure under both stress- and strain-controlled methods, as both approaches have been used frequently and interchangeably in experimental and computational studies [79]. As such, the improved bulk AF tensile mechanical properties with AGE accumulation were achieved at the risk of exposing the extrafibrillar matrix to increased mechanical damage accumulation. Additionally, previous cellular biology studies showed that higher stresses applied to AF cells caused inflammatory responses, which may also trigger premature tissue failure through catabolic remodeling [80-82]. Lastly, future experimental work is needed to confirm that findings from this study are translatable to human disc tissues.

The biaxial boundary condition was simulated in the current study due to its physiologic relevance and difficulties in conducting repeatable soft tissue biaxial tensile testing in vitro. Model predictions highlighted that glycation had a greater effect on AF bulk and subtissue-level mechanics than the evaluated biaxial boundary condition (i.e., an axial-fixed condition), especially on the stresses in the extrafibrillar matrix (**Figure 8B**). However, the more constrained biaxial boundary amplified the effect of glycation, disposing nearly all the matrix elements in the GLY50 biaxial model to failure under large physiologic deformations (**Figure 8C**). This amplifying effect may be more pronounced in vivo, as the heavily glycated tissues would be more restricted by the surrounding structures (e.g., the nucleus and endplates), further increasing the risk of tissue failure.

One limitation of the current study was that tissue proteoglycan content was not characterized. However, previous in vitro studies consistently reported that AGE treatment did not affect proteoglycan content, regardless of the crosslinking agent used [83-85]. Tissue water content, a benchmark for proteoglycan content, also remained at the fresh tissue level for all treatment groups (**Figure 5B**), suggesting that proteoglycan was unaffected by the methylglyoxal-based treatment. While AGE content in discs from diabetic patients has not been characterized, the AGE content induced in GLY25 specimens aligned well with the range measured from human cadaveric disc tissues, while CTRL and GLY50 specimens covered the lower and higher end of that range (**Figure 5A**) [20], making our specimens justifiable candidate tissue models to examine the differences between healthy and diabetic tissues. Another limitation was that the current study did not characterize the elastin-derived AGE content, which could have a considerable effect on AF mechanics, especially with degeneration [59]. Computationally, crosslinks were described as extrafibrillar reinforcements. Future models may need to explicitly describe crosslinks to differentiate failure originating from the extrafibrillar matrix from the crosslinks themselves, as well as to understand the relative contribution of fiber stiffening and reduced interfibrillar sliding to bulk tissue strengthening with glycation, which remains a debate in the field [69, 70, 72, 78].

4. Conclusions

The current study evaluated the effects of AGEs on anisotropic AF uniaxial tensile mechanics using a combined experimental-computational approach. Experimentally, AF uniaxial tensile mechanical properties were reported in circumferential-radial and radial directions at three physiologically relevant AGE levels. Computationally, multiscale structure-based FEMs were developed and validated to describe crosslinks within the extrafibrillar matrix. The validated models were used to examine the effect of glycation on multiscale AF mechanics under uniaxial

and biaxial boundary conditions. Mechanical testing results showed that in vitro glycation did not lead to compromised AF mechanical properties under monotonic quasistatic uniaxial tension in both tested orientations, agreeing with previous literature. The proposed FEM framework accurately predicted AF bulk tensile mechanics with glycation and provided insight into the relationship between AGE accumulation and more frequent and severe tissue failure observed with diabetes. Specifically, glycation exposed the extrafibrillar matrix to greater stresses under physiologically relevant deformations, which may lead to increased tissue failure through greater accumulated mechanical damage or catabolic tissue remodeling. Our findings also suggested probable crosslinking structures at the subtissue level, indicating that AGEs had a more pronounced effect along the fiber direction, while interlamellar radial crosslinks were less likely to form in the AF. In conclusion, the improved bulk mechanical properties of fiber-reinforced biological tissues with AGE accumulation may be achieved at the risk of exposing the extrafibrillar matrix to larger stresses under physiologic deformations, leading to premature tissue failure. The presented combined approach provides a powerful tool for examining multiscale AF structure-function relationships with disease progression, which is crucial for developing effective preventive measures and therapeutic interventions for low back pain.

5. Acknowledgements

Funding: This work was supported by National Science Foundation [CAREER #1751212 – GDO; GRFP #DGE 2146752 – ESA].

This material is based upon work supported by the National Science Foundation Graduate Research Fellowship Program under Grant No. DGE 2146752. Any opinions, findings, and conclusions or recommendations expressed in this material are those of the author(s) and do not necessarily reflect the views of the National Science Foundation.

References

[1] Hoy, D., March, L., Brooks, P., Blyth, F., Woolf, A., Bain, C., Williams, G., Smith, E., Vos, T., Barendregt, J. and Murray, C., 2014. The global burden of low back pain: estimates from the Global Burden of Disease 2010 study. Annals of the rheumatic diseases, 73(6), pp.968-974.

[2] Bloom, D.E., Boersch-Supan, A., McGee, P. and Seike, A., 2011. Population aging: facts, challenges, and responses. Benefits and compensation International, 41(1), p.22.

[3] Popkin, B.M., 2015. Nutrition transition and the global diabetes epidemic. Current diabetes reports, 15, pp.1-8.

[4] Zhou, B., Lu, Y., Hajifathalian, K., Bentham, J., Di Cesare, M., Danaei, G., Bixby, H., Cowan, M.J., Ali, M.K., Taddei, C. and Lo, W.C., 2016. Worldwide trends in diabetes since 1980: a pooled analysis of 751 population-based studies with 4· 4 million participants. The lancet, 387(10027), pp.1513-1530.

[5] Jakoi, A.M., Pannu, G., D'oro, A., Buser, Z., Pham, M.H., Patel, N.N., Hsieh, P.C., Liu, J.C., Acosta, F.L., Hah, R. and Wang, J.C., 2017. The clinical correlations between diabetes, cigarette smoking and obesity on intervertebral degenerative disc disease of the lumbar spine. Asian spine journal, 11(3), p.337.

[6] Liu, X., Pan, F., Ba, Z., Wang, S. and Wu, D., 2018. The potential effect of type 2 diabetes mellitus on lumbar disc degeneration: a retrospective single-center study. Journal of Orthopaedic Surgery and Research, 13(1), pp.1-5.

[7] Steelman, T., Lewandowski, L., Helgeson, M., Wilson, K., Olsen, C. and Gwinn, D., 2018. Population-based risk factors for the development of degenerative disk disease. Clinical spine surgery, 31(8), pp.E409-E412.

[8] Russo, F., Ambrosio, L., Ngo, K., Vadalà, G., Denaro, V., Fan, Y., Sowa, G., Kang, J.D. and Vo, N., 2019. The role of type I diabetes in intervertebral disc degeneration. Spine, 44(17), p.1177.

[9] Jhawar, B.S., Fuchs, C.S., Colditz, G.A. and Stampfer, M.J., 2006. Cardiovascular risk factors for physician-diagnosed lumbar disc herniation. The spine journal, 6(6), pp.684-691.

[10] Raj, P.P., 2008. Intervertebral disc: anatomy‐physiology‐pathophysiology‐treatment. Pain Practice, 8(1), pp.18-44.

[11] Adams, M.A. and Roughley, P.J., 2006. What is intervertebral disc degeneration, and what causes it?. Spine, 31(18), pp.2151-2161.

[12] Vergroesen, P.P., Kingma, I., Emanuel, K.S., Hoogendoorn, R.J., Welting, T.J., van Royen, B.J., van Dieën, J.H. and Smit, T.H., 2015. Mechanics and biology in intervertebral disc degeneration: a vicious circle. Osteoarthritis and cartilage, 23(7), pp.1057-1070.

[13] Vlassara, H. and Palace, M.R., 2002. Diabetes and advanced glycation endproducts. Journal of internal medicine, 251(2), pp.87-101.

[14] Ahmed, N. and Thornalley, P.J., 2007. Advanced glycation endproducts: what is their relevance to diabetic complications?. Diabetes, Obesity and Metabolism, 9(3), pp.233-245.

[15] Suzuki, A., Yabu, A. and Nakamura, H., 2022. Advanced glycation end products in musculoskeletal system and disorders. Methods, 203, pp.179-186.

[16] Verzijl, N., DeGroot, J., Thorpe, S.R., Bank, R.A., Shaw, J.N., Lyons, T.J., Bijlsma, J.W., Lafeber, F.P., Baynes, J.W. and TeKoppele, J.M., 2000. Effect of collagen turnover on the accumulation of advanced glycation end products. Journal of Biological Chemistry, 275(50), pp.39027-39031.

[17] Snedeker, J.G. and Gautieri, A., 2014. The role of collagen crosslinks in ageing and diabetes-the good, the bad, and the ugly. Muscles, ligaments and tendons journal, 4(3), p.303.

[18] Wagner, D.R., Reiser, K.M. and Lotz, J.C., 2006. Glycation increases human annulus fibrosus stiffness in both experimental measurements and theoretical predictions. Journal of biomechanics, 39(6), pp.1021-1029.

[19] Chuang, S.Y., Odono, R.M. and Hedman, T.P., 2007. Effects of exogenous crosslinking on in vitro tensile and compressive moduli of lumbar intervertebral discs. Clinical Biomechanics, 22(1), pp.14-20.

[20] Werbner, B., Lee, M., Lee, A., Yang, L., Habib, M., Fields, A.J. and O'Connell, G.D., 2022. Non-enzymatic glycation of annulus fibrosus alters tissue-level failure mechanics in tension. Journal of the Mechanical Behavior of Biomedical Materials, 126, p.104992.

[21] Hedman, T.P., Saito, H., Vo, C. and Chuang, S.Y., 2006. Exogenous cross-linking increases the stability of spinal motion segments. Spine, 31(15), pp.E480-E485.

[22] Barbir, A., Michalek, A.J., Abbott, R.D. and Iatridis, J.C., 2010. Effects of enzymatic digestion on compressive properties of rat intervertebral discs. Journal of biomechanics, 43(6), pp.1067-1073.

[23] Kirking, B.C., Toungate, J.K. and Hedman, T.P., 2013. The dose response relationship between intervertebral disc flexion-extension neutral zone metrics and injected genipin concentration. Journal of applied biomaterials & functional materials, 11(2), pp.73-79.

[24] Fields, A.J., Berg-Johansen, B., Metz, L.N., Miller, S., La, B., Liebenberg, E.C., Coughlin, D.G., Graham, J.L., Stanhope, K.L., Havel, P.J. and Lotz, J.C., 2015. Alterations in intervertebral disc composition, matrix homeostasis and biomechanical behavior in the UCD-T2DM rat model of type 2 diabetes. Journal of orthopaedic research, 33(5), pp.738-746.

[25] Krishnamoorthy, D., Hoy, R.C., Natelson, D.M., Torre, O.M., Laudier, D.M., Iatridis, J.C. and Illien-Jünger, S., 2018. Dietary advanced glycation end-product consumption leads to mechanical stiffening of murine intervertebral discs. Disease Models & Mechanisms, 11(12), p.dmm036012.

[26] Werbner, B., Zhou, M. and O'Connell, G., 2017. A novel method for repeatable failure testing of annulus fibrosus. Journal of biomechanical engineering, 139(11).

[27] Werbner, B., Zhou, M., McMindes, N., Lee, A., Lee, M. and O'Connell, G.D., 2022. Saline-polyethylene glycol blends preserve in vitro annulus fibrosus hydration and mechanics: An experimental and finite-element analysis. Journal of the Mechanical Behavior of Biomedical Materials, 125, p.104951.

[28] Zhou, M., Bezci, S.E. and O'Connell, G.D., 2020. Multiscale composite model of fiber-reinforced tissues with direct representation of sub-tissue properties. Biomechanics and Modeling in Mechanobiology, 19, pp.745-759.

[29] Zhou, M., Werbner, B. and O'Connell, G.D., 2021. Fiber engagement accounts for geometry-dependent annulus fibrosus mechanics: A multiscale, Structure-Based Finite Element Study. journal of the mechanical behavior of biomedical materials, 115, p.104292.

[30] Zhou, M., Lim, S. and O'Connell, G.D., 2021. A robust multiscale and multiphasic structure-based modeling framework for the intervertebral disc. Frontiers in Bioengineering and Biotechnology, 9, p.685799.

[31] Zhou, M., Huff, R.D., Abubakr, Y. and O'Connell, G.D., 2022. Torque-and muscle-driven flexion induce disparate risks of in vitro herniation: A multiscale and multiphasic structure-based finite element study. Journal of biomechanical engineering, 144(6), p.061005.

[32] Demers, C.N., Antoniou, J. and Mwale, F., 2004. Value and limitations of using the bovine tail as a model for the human lumbar spine. Spine, 29(24), pp.2793-2799.

[33] O'Connell, G.D., Vresilovic, E.J. and Elliott, D.M., 2007. Comparison of animals used in disc research to human lumbar disc geometry. Spine, 32(3), pp.328-333.

[34] Bezci, S.E., Werbner, B., Zhou, M., Malollari, K.G., Dorlhiac, G., Carraro, C., Streets, A. and O'Connell, G.D., 2019. Radial variation in biochemical composition of the bovine caudal intervertebral disc. Jor Spine, 2(3), p.e1065.

[35] Yu, J., Tirlapur, U., Fairbank, J., Handford, P., Roberts, S., Winlove, C.P., Cui, Z. and Urban, J., 2007. Microfibrils, elastin fibres and collagen fibres in the human intervertebral disc and bovine tail disc. Journal of anatomy, 210(4), pp.460-471.

[36] Taylor, D., O'Mara, N., Ryan, E., Takaza, M. and Simms, C., 2012. The fracture toughness of soft tissues. Journal of the mechanical behavior of biomedical materials, 6, pp.139-147.

[37] Hollander, A.P., Heathfield, T.F., Webber, C., Iwata, Y., Bourne, R., Rorabeck, C. and Poole, A.R., 1994. Increased damage to type II collagen in osteoarthritic articular cartilage detected by a new immunoassay. The Journal of clinical investigation, 93(4), pp.1722-1732.

[38] Marchand, F. and Ahmed, A.M., 1990. Investigation of the laminate structure of lumbar disc anulus fibrosus. Spine, 15(5), pp.402-410.

[39] Schollum, M.L., Robertson, P.A. and Broom, N.D., 2010. How age influences unravelling morphology of annular lamellae–a study of interfibre cohesivity in the lumbar disc. Journal of anatomy, 216(3), pp.310-319.

[40] Holzapfel, G.A., Schulze-Bauer, C.A., Feigl, G. and Regitnig, P., 2005. Single lamellar mechanics of the human lumbar anulus fibrosus. Biomechanics and modeling in mechanobiology, 3, pp.125-140.

[41] Matcher, S.J., Winlove, C.P. and Gangnus, S.V., 2004. The collagen structure of bovine intervertebral disc studied using polarization-sensitive optical coherence tomography. Physics in Medicine & Biology, 49(7), p.1295.

[42] Maas, S.A., Ellis, B.J., Ateshian, G.A. and Weiss, J.A., 2012. FEBio: finite elements for biomechanics.

[43] Lai, W.M., Hou, J.S. and Mow, V.C., 1991. A triphasic theory for the swelling and deformation behaviors of articular cartilage.

[44] Urban, J.P.G. and Maroudas, A., 1979. The measurement of fixed charged density in the intervertebral disc. Biochimica et Biophysica Acta (BBA)-General Subjects, 586(1), pp.166-178.

[45] Antoniou, J., Steffen, T., Nelson, F., Winterbottom, N., Hollander, A.P., Poole, R.A., Aebi, M. and Alini, M., 1996. The human lumbar intervertebral disc: evidence for changes in the biosynthesis and denaturation of the extracellular matrix with growth, maturation, ageing, and degeneration. The Journal of clinical investigation, 98(4), pp.996-1003.

[46] Cao, L., Guilak, F. and Setton, L.A., 2009. Pericellular matrix mechanics in the anulus fibrosus predicted by a three-dimensional finite element model and in situ morphology. Cellular and molecular bioengineering, 2, pp.306-319.

[47] Périé, D., Korda, D. and Iatridis, J.C., 2005. Confined compression experiments on bovine nucleus pulposus and annulus fibrosus: sensitivity of the experiment in the determination of compressive modulus and hydraulic permeability. Journal of biomechanics, 38(11), pp.2164-2171.

[48] Pham, D.T., Shapter, J.G. and Costi, J.J., 2018. Tensile behaviour of individual fibre bundles in the human lumbar anulus fibrosus. Journal of biomechanics, 67, pp.24-31.

[49] Grömping, U., 2007. Relative importance for linear regression in R: the package relaimpo. Journal of statistical software, 17, pp.1-27.

[50] Heuer, F., Schmidt, H. and Wilke, H.J., 2008. The relation between intervertebral disc bulging and annular fiber associated strains for simple and complex loading. Journal of biomechanics, 41(5), pp.1086-1094.

[51] O'Connell, G.D., Vresilovic, E.J. and Elliott, D.M., 2011. Human intervertebral disc internal strain in compression: the effect of disc region, loading position, and degeneration. Journal of orthopaedic research, 29(4), pp.547-555.

[52] Skaggs, D.L., Weidenbaum, M., Iatridis, J.C., Ratcliffe, A. and Mow, V.C., 1994. Regional variation in tensile properties and biochemical composition of the human lumbar anulus fibrosus. Spine, 19(12), pp.1310-1319.

[53] Acaroglu, E.R., Latridis, J.C., Setton, L.A., Foster, R.J., Mow, V.C. and Weidenbaum, M., 1995. Degeneration and aging affect the tensile behavior of human lumbar anulus fibrosus. Spine, 20(24), pp.2690-2701.

[54] Fujita, Y., Duncan, N.A. and Lotz, J.C., 1997. Radial tensile properties of the lumbar annulus fibrosus are site and degeneration dependent. Journal of orthopaedic research, 15(6), pp.814-819.

[55] Elliott, D.M. and Setton, L.A., 2001. Anisotropic and inhomogeneous tensile behavior of the human anulus fibrosus: experimental measurement and material model predictions. J. Biomech. Eng., 123(3), pp.256-263.

[56] O'Connell, G.D., Guerin, H.L. and Elliott, D.M., 2009. Theoretical and uniaxial experimental evaluation of human annulus fibrosus degeneration.

[57] Adams, M.A. and Green, T.P., 1993. Tensile properties of the annulus fibrosus: I. The contribution of fibre-matrix interactions to tensile stiffness and strength. European Spine Journal, 2, pp.203-208.

[58] Cloyd, J.M. and Elliott, D.M., 2007. Elastin content correlates with human disc degeneration in the anulus fibrosus and nucleus pulposus. Spine, 32(17), pp.1826-1831.

[59] Smith, L.J. and Fazzalari, N.L., 2009. The elastic fibre network of the human lumbar anulus fibrosus: architecture, mechanical function and potential role in the progression of intervertebral disc degeneration. European Spine Journal, 18, pp.439-448.

[60] Cyril, D., Giugni, A., Bangar, S.S., Mirzaeipoueinak, M., Shrivastav, D., Sharabi, M., Tipper, J.L. and Tavakoli, J., 2022. Elastic fibers in the intervertebral disc: From form to function and toward regeneration. International Journal of Molecular Sciences, 23(16), p.8931.

[61] Tseng, J.Y., Ghazaryan, A.A., Lo, W., Chen, Y.F., Hovhannisyan, V., Chen, S.J., Tan, H.Y. and Dong, C.Y., 2011. Multiphoton spectral microscopy for imaging and quantification of tissue glycation. Biomedical optics express, 2(2), pp.218-230.

[62] Ebara, S., Iatridis, J.C., Setton, L.A., Foster, R.J., Mow, V.C. and Weidenbaum, M., 1996. Tensile properties of nondegenerate human lumbar anulus fibrosus. Spine, 21(4), pp.452-461.

[63] Thompson, J.P., Pearce, R.H., Schechter, M.T., Adams, M.E., Tsang, I.K. and Bishop, P.B., 1990. Preliminary evaluation of a scheme for grading the gross morphology of the human intervertebral disc. Spine, 15(5), pp.411-415.

[64] Handl, M.I.L.A.N., Filova, E., Kubala, M., Lánský, Z., Koláčná, L., Vorlíček, J., Trč, T., Pach, M. and Amler, E., 2007. Fluorescent advanced glycation end products in the detection of factual stages of cartilage degeneration. Physiological research, 56(2).

[65] Lui, P.P.Y., 2017. Tendinopathy in diabetes mellitus patients—epidemiology, pathogenesis, and management. Scandinavian journal of medicine & science in sports, 27(8), pp.776-787.

[66] de Oliveira, R.R., de Lira, K.D.S., de Castro Silveira, P.V., Coutinho, M.P.G., Medeiros, M.N., Teixeira, M.F.H.B.I. and de Moraes, S.R.A., 2011. Mechanical properties of achilles tendon in rats induced to experimental diabetes. Annals of biomedical engineering, 39, pp.1528-1534.

[67] Fox, A.J., Bedi, A., Deng, X.H., Ying, L., Harris, P.E., Warren, R.F. and Rodeo, S.A., 2011. Diabetes mellitus alters the mechanical properties of the native tendon in an experimental rat model. Journal of Orthopaedic Research, 29(6), pp.880-885.

[68] Avila, M.Y. and Navia, J.L., 2010. Effect of genipin collagen crosslinking on porcine corneas. Journal of Cataract & Refractive Surgery, 36(4), pp.659-664.

[69] Li, Y., Fessel, G., Georgiadis, M. and Snedeker, J.G., 2013. Advanced glycation end-products diminish tendon collagen fiber sliding. Matrix Biology, 32(3-4), pp.169-177.

[70] Gautieri, A., Passini, F.S., Silván, U., Guizar-Sicairos, M., Carimati, G., Volpi, P., Moretti, M., Schoenhuber, H., Redaelli, A., Berli, M. and Snedeker, J.G., 2017. Advanced glycation end-products: Mechanics of aged collagen from molecule to tissue. Matrix Biology, 59, pp.95-108.

[71] Reddy, G.K., Stehno-Bittel, L. and Enwemeka, C.S., 2002. Glycation-induced matrix stability in the rabbit achilles tendon. Archives of biochemistry and biophysics, 399(2), pp.174-180.

[72] Svensson, R.B., Smith, S.T., Moyer, P.J. and Magnusson, S.P., 2018. Effects of maturation and advanced glycation on tensile mechanics of collagen fibrils from rat tail and Achilles tendons. Acta biomaterialia, 70, pp.270-280.

[73] McGann, M.E., Bonitsky, C.M., Jackson, M.L., Ovaert, T.C., Trippel, S.B. and Wagner, D.R., 2015. Genipin crosslinking of cartilage enhances resistance to biochemical degradation and mechanical wear. Journal of Orthopaedic Research®, 33(11), pp.1571-1579.

[74] Yoshida, T., Park, J.S., Yokosuka, K., Jimbo, K., Yamada, K., Sato, K., Takeuchi, M., Yamagishi, S.I. and Nagata, K., 2009. Up-regulation in receptor for advanced glycation end-products in inflammatory circumstances in bovine coccygeal intervertebral disc specimens in vitro. Spine, 34(15), pp.1544-1548.

[75] Hu, Y., Shao, Z., Cai, X., Liu, Y., Shen, M., Yao, Y., Yuan, T., Wang, W., Ding, F. and Xiong, L., 2019. Mitochondrial pathway is involved in advanced glycation end products-induced apoptosis of rabbit annulus fibrosus cells. Spine, 44(10), p.E585.

[76] Hoy, R.C., D'Erminio, D.N., Krishnamoorthy, D., Natelson, D.M., Laudier, D.M., Illien-Jünger, S. and Iatridis, J.C., 2020. Advanced glycation end products cause RAGE-dependent annulus fibrosus collagen disruption and loss identified using in situ second harmonic generation imaging in mice intervertebral disk in vivo and in organ culture models. JOR spine, 3(4), p.e1126.

[77] Illien-Junger, S., Grosjean, F., Laudier, D.M., Vlassara, H., Striker, G.E. and Iatridis, J.C., 2013. Combined anti-inflammatory and anti-AGE drug treatments have a protective effect on intervertebral discs in mice with diabetes. PLoS One, 8(5), p.e64302.

[78] Fessel, G., Li, Y., Diederich, V., Guizar-Sicairos, M., Schneider, P., Sell, D.R., Monnier, V.M. and Snedeker, J.G., 2014. Advanced glycation end-products reduce collagen molecular sliding to affect collagen fibril damage mechanisms but not stiffness. PloS one, 9(11), p.e110948.

[79] Costi, J.J., Ledet, E.H. and O'Connell, G.D., 2021. Spine biomechanical testing methodologies: the controversy of consensus vs scientific evidence. JOR spine, 4(1), p.e1138.

[80] Rannou, F., Richette, P., Benallaoua, M., François, M., Genries, V., Korwin-Zmijowska, C., Revel, M., Corvol, M. and Poiraudeau, S., 2003. Cyclic tensile stretch modulates proteoglycan production by intervertebral disc annulus fibrosus cells through production of nitrite oxide. Journal of cellular biochemistry, 90(1), pp.148-157.

[81] Gawri, R., Rosenzweig, D.H., Krock, E., Ouellet, J.A., Stone, L.S., Quinn, T.M. and Haglund, L., 2014. High mechanical strain of primary intervertebral disc cells promotes secretion of inflammatory factors associated with disc degeneration and pain. Arthritis research & therapy, 16(1), pp.1-14.

[82] Dombrowski, M.E., Olsen, A.S., Vaudreuil, N., Couch, B.K., Dong, Q., Tucci, M., Lee, J.Y., Vo, N.V. and Sowa, G., 2020. Rabbit annulus fibrosus cells express neuropeptide Y, which is influenced by mechanical and inflammatory stress. Neurospine, 17(1), p.69.

[83] Yerramalli, C.S., Chou, A.I., Miller, G.J., Nicoll, S.B., Chin, K.R. and Elliott, D.M., 2007. The effect of nucleus pulposus crosslinking and glycosaminoglycan degradation on disc mechanical function. Biomechanics and modeling in mechanobiology, 6, pp.13-20.

[84] Jazini, E., Sharan, A.D., Morse, L.J., Dyke, J.P., Aronowitz, E.A., Chen, L.K. and Tang, S.Y., 2012. Alterations in magnetic resonance imaging T2 relaxation times of the ovine intervertebral disc due to non-enzymatic glycation. Spine, 37(4), p.E209.

[85] Liu, J.W., Abraham, A.C. and Tang, S.Y., 2015. The high-throughput phenotyping of the viscoelastic behavior of whole mouse intervertebral discs using a novel method of dynamic mechanical testing. Journal of biomechanics, 48(10), pp.2189-2194.